electronics

Article

Optimal Sliding Speed and Contact Pressure Design of On-Load Tap Changer Based on Multivariate Nonlinear Regression

Zhiqi Xu [1], Sijiang Zhang [1], Jintao Zhang [1], Xiaobing Wang [1], Yanwen Xu [1], Zongying Li [2], Minghan Ma [2] and Shuaibing Li [2,*]

[1] GanSu Guangming Electric Power Engineering Consulting and Supervision Co., Ltd., Lanzhou 730050, China; 18919158706@163.com (Z.X.); 13919122027@163.com (S.Z.); zhangjt0765@163.com (J.Z.); wxbinglove@163.com (X.W.); 18794808969@163.com (Y.X.)
[2] School of New Energy and Power Engineering, Lanzhou Jiaotong University, Lanzhou 730070, China; lizongying1998@163.com (Z.L.); maminghan0228@163.com (M.M.)
* Correspondence: shuaibingli@mail.lzjtu.cn; Tel.: +86-13919490494

Abstract: During the voltage regulation of on-load tap changers (OLTCs), the movement of the contacts can easily cause arcing, which may lead to erosion or malfunction. To reduce the energy and probability of arcing, we focus on designing an optimal range for the sliding speed and contact pressure of the contacts to minimize arc energy. Initially, our research introduces a novel OLTC arc testing platform to simulate the motion of static and dynamic contacts, exploring the relationship between different sliding speeds, contact pressures, and factors like arc voltage waveform, arcing rate, arc resistance, and arc energy. Subsequently, by employing multiple nonlinear regression methods, we establish functional relationships between sliding speed and arc energy, as well as contact pressure and arc energy, evaluating the fit using correlation coefficients. Finally, through analyzing their nonlinear behaviors, we determine the ideal sliding speed and contact pressure. The results indicate that when the OLTC contacts slide at an optimal speed between 89 and 103 mm/s and optimal contact pressure between 1.5 and 1.7 N, the arc energy can be minimized, thereby enhancing the performance and lifespan of the on-load tap changer. This study offers feasible insights for the design and operation of OLTCs, aiding in the improvement of power system regulation.

Keywords: oil-immersed OLTC; sliding speed; contact pressure; arc energy; multiple nonlinear regression

Citation: Xu, Z.; Zhang, S.; Zhang, J.; Wang, X.; Xu, Y.; Li, Z.; Ma, M.; Li, S. Optimal Sliding Speed and Contact Pressure Design of On-Load Tap Changer Based on Multivariate Nonlinear Regression. *Electronics* **2024**, *13*, 4349. https://doi.org/10.3390/electronics13224349

Academic Editor: Ahmed Abu-Siada

Received: 6 October 2024
Revised: 31 October 2024
Accepted: 1 November 2024
Published: 6 November 2024

1. Introduction

In recent years, new energy-based power systems have developed rapidly, but due to their randomness and volatility, having a high proportion of new energy sources connected to the grid is prone to cause surge and voltage fluctuations, which reduces the power quality. An on-load voltage regulator transformer ensures the stability of voltage at the user side through the step-by-step switching of dynamic and static contacts and plays an important role in contacting the power grid, regulating active and reactive currents and maintaining voltage stability [1–5]. As the only movable part in the transformer, the action frequency of the on-load tap changer increases with the demand of grid regulation, but the wear and abrasion induced by arcing between contacts will reduce its service life and affect the stability of the grid [6,7].

The core of studying the arc damage problem lies in studying the current-carrying friction wear. For this reason, many researchers and scholars at home and abroad have built simulation experimental devices, mainly from the current, contact pressure and sliding speed and other aspects of the study, and achieved significant results.

In the study of the effect of an electric current on friction wear, the current change affects friction wear in a complex way by inducing the magnetic field change and magnetohydrodynamic effect, changing the temperature of the friction surface and its material properties (e.g., hardness, strength, and lubrication performance), and promoting an electrochemical reaction (e.g., corrosion and oxidation). L. Dong et al. [8] based on the bow network arc test system, studied the volt-ampere characteristics of the high-speed railroad bow network system arc discharge and found that the stable arc-firing voltage with an increase in the current was slightly reduced, while the slope of the arc-firing spike voltage changes with an increase in current and increased. L. Dong, W. Fu et al. [9,10] used a pin–disk friction wear testing machine and studied a subway power supply steel–aluminum composite rail and a receiving boot in the presence or absence of electricity under the sliding friction wear, finding that the current existed when the wear significantly increased and a high current led to material softening, aggravated by electrical ablation wear. Z. Xing et al. [11], through the high-speed current-carrying friction and wear test, found that the low voltage and high current conditions of a short-arc discharge increase wear, the carbon slider manifested as arc ablation, stripping, melting and vaporization, and the friction factor first increased and then decreased. C. Zhong et al. [12] analyzed the effects of current intensity, sliding speed, and pressure fluctuation on the wear rate by strong current sliding electrical contact experiments. T. Ding et al. [13] simulated the subway bow network to study the wear performance of an immersed metal–carbon sliding plate under 200–400 A direct current, 15–40 N normal load, and 40–120 km/h sliding speed and found differences in temperature changes and wear mechanisms under different current conditions.

For the effect of contact pressure on frictional wear, T. Ding, G. Shi et al. [14–16] investigated the frictional wear of stainless steel/impregnated metal–carbon carriers under different normal loads by means of a pin–disk testing machine and found that the friction coefficient decreased with an increase in load up to 160 N and then tended to stabilize. Z. Chen, S. Zhang, S. Wang, X. Wang et al. [17–20] investigated the effect of fluctuating load on the contact resistance of the bow network by using a sliding electrical contact experimental machine and established a prediction model. Z. Chen et al. [21] studied the AuNi9/gold-plated friction pair and found that the friction factor was first high and then low at high loads. S. Wang, S. Zhang et al. [18,19] studied the frictional vibration of the sliding electrical contact of a bow mesh under fluctuating load by regression modeling. X. Wang et al. [20] investigates the effect of load on the stability of an AuNi9/PdNi-Au friction pair. Z. Chen, C. Qu et al. [21,22] investigated the carrier friction wear of immersed metal–carbon sliding plates under different loads and found that the friction factor increased with increasing load.

In order to investigate the effect of current-carrying conditions on the friction and wear properties of copper-carbon composite materials, X. Yu et al. [23] found that the load significantly affects the current-carrying friction and wear performance, as well as the stability of the AuNi9/PdNi-Au friction pair, revealing distinct wear mechanisms at different load levels. D. Liu et al. [24] found that increasing the normal force on metal-impregnated carbon strips enhances current-carrying efficiency and reduces wear by mitigating arc ablation effects, while also stabilizing the wear rate over extended sliding distances. Z. Yang et al. [25] found that copper-graphite horizontal gradient composites can effectively manage friction damage by optimizing graphite content at different locations on the friction surface, enhancing lubrication and conductivity while reducing wear and arc damage during current-carrying friction processes. B. Dong et al. [26] found that during current-carrying friction in pantograph-catenary systems, increasing normal contact force suppresses arc discharge energy and temperature rise of carbon strips, while higher electric current and sliding speed lead to increased arc discharge energy and temperature rise.

In order to investigate the effect of sliding speed on frictional wear, H. Yang et al. [27] found that an increase in the current and sliding speed led to an increase in arc discharge energy and a temperature rise in pure carbon sliding plates. Z. Liu et al. [28] showed that an increase in the sliding speed resulted in increased frictional oscillations in the contact strip and contact line and increased arc discharge and ablation. A study by J. Li et al. [29] showed that an increase in sliding velocity led to a decrease in the friction factor and an increase in the wear rate in the presence of an applied current. D. Wang et al. [30] have found that the initial arc formation time is advanced and the arc ignition rate and arc energy increase at high speeds. X. Luo et al. [31] showed that an increase in the sliding speed led to a rise and then a fall in the friction coefficient, along with an increase in the contact voltage drop.

In summary, the existing arc research is mainly focused on the air medium, and regarding the discharge mechanism in the transformer oil medium, there is still insufficient research. There are two problems in this type of research: one is the lack of clear and quantitative factors affecting the arc in the transformer oil medium, and the second is that most of the sliding of the OLTC contact is designed and used based on experience, and there is a lack of research on the sliding speed for the maximization of arc suppression. The arc discharge behavior in the transformer oil medium is affected by a variety of factors such as the dielectric properties and thermal conductivity of the medium. Arc discharge behavior refers to the electrical breakdown of a gas that produces a prolonged electrical discharge. This phenomenon occurs when the voltage across a gap exceeds the dielectric strength of the medium, leading to a conductive path through which a current flows. In the context of on-load tap changers (OLTCs), understanding arc discharge behavior is crucial as it affects the wear and performance of the contacts, impacting the overall stability and efficiency of power systems. It is urgent to explore the impact of different factors in the oil medium on the arc suppression to complete the design of the optimal sliding speed of the OLTC.

In view of the above problems, the primary objective of this study is to investigate the arc discharge behavior in oil-immersed OLTCs, focusing on the effects of sliding speed and contact pressure on arc characteristics. By employing multiple nonlinear regression analysis, the study aims to identify the optimal operating conditions that minimize arc energy, thereby enhancing the performance and lifespan of OLTCs. This research goes beyond a parametric study by providing actionable insights for the design and operation of OLTCs, contributing to an improvement in existing methods in power system regulation.

The main innovative contributions of this article are as follows:

1. This study builds an arc test platform that can simulate the contact mode of OLTC movable/static contacts. This platform allows for the precise control of sliding speed and contact pressure, enabling the study of arc characteristics under realistic conditions. The insights gained from this setup can be directly applied to actual engineering applications, providing a reference for material selection, shape design, and operation specifications of OLTC contacts.
2. The research employs multiple nonlinear regression analysis to identify optimal operating conditions that minimize arc energy, thereby enhancing the performance and lifespan of OLTCs. This provides a significant advancement in improving existing power system regulation methods.

2. Materials and Methods

2.1. OLTC Arc Test Platform

In order to simulate the contact pattern between the moving and static contacts in an oil-immersed load-regulated transformer (OLTC), an OLTC friction and wear test setup is designed in this paper, as shown in Figure 1. The device mainly includes a regulator, a transformer, a protective resistor, a voltage divider, an oscilloscope and OLTC friction and wear test equipment. The inverter motor drives the contact sliding through the guide rail, and the sliding speed of the contact is adjusted by an intelligent control system in the range of 0–120 mm/s to simulate the working condition under different sliding speeds. By adjusting the tightness of the nut, a contact pressure of 0–2 N can be applied between the contacts to ensure stable contact during the test. The configuration of relevant parameters of the arc experiment platform is shown in Table 1.

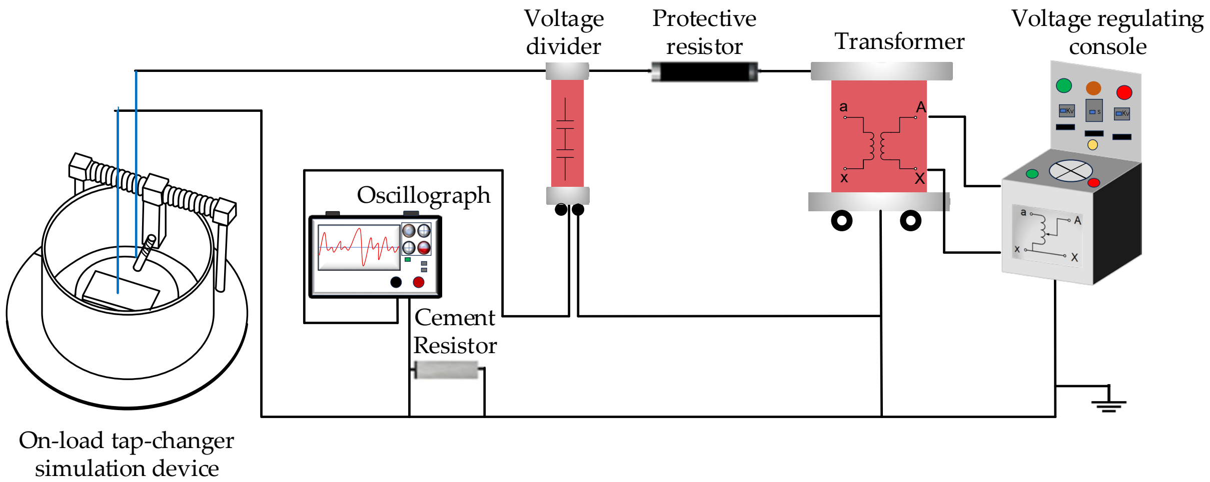

Figure 1. OLTC arc experiment platform.

Table 1. Arc experiment platform parameter configuration table.

Name	Parameter Name	Detailed Parameter
Contact regulator	input voltage output voltage electrical strength insulation resistance	single-phase 220 V, three-phase (three-phase four-wire) 380 V, single-phase 0–250, three-phase 0–430 2000 V/min single-phase > 50 MΩ three-phase > 2 MΩ
Transformer	rated capacity rated voltage rated current cooling method	50 kVA 0.4/100 kV 125/0.5 A ONAN
Transformer oil	model	Karamay 25 mineral oil

2.2. OLTC's Control and Measurement System

The control system of the test equipment, shown in Figure 2, integrates advanced technologies, including a K series intelligent motion controller panel, PLC industrial control panel and stepper motor driver. The K series controller panel adopts PID control algorithms to realize the real-time adjustment of motor speed and position. The PLC panel provides flexible input/output interfaces to configure the sensors and actuators to the ensure coordinated operation of the equipment. The stepper motor driver adjusts the direction of the rotation, step and speed of the motor according to the control signal, number of pulses and frequency, thus realizing precise control and stable operation.

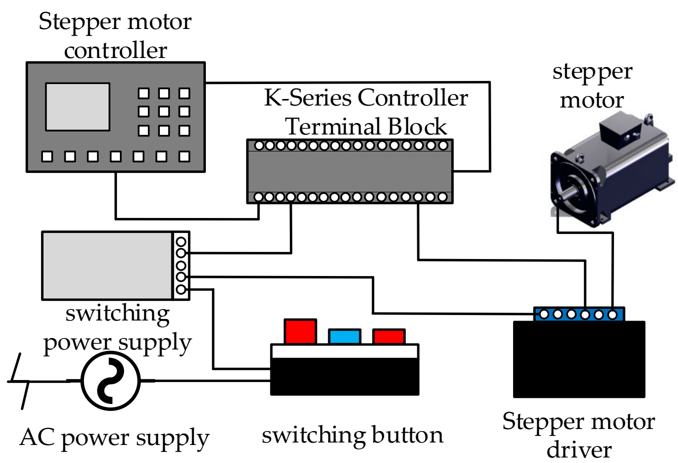

Figure 2. Control system for OLTC.

2.3. OLTC Arc Testing Program Design

2.3.1. Preparation of Experimental Materials

The test materials are shown in Table 2, and copper–tungsten materials are selected for the contacts, as shown in Figure 3. Before each test, the contact surface was sandpapered to ensure consistency. To ensure consistency in the contact surface preparation, sandpaper with a grit size of 600 was used uniformly across all test samples. The sandpaper was replaced after every 10 samples to maintain its abrasiveness and ensure a consistent surface roughness. This standardized approach minimizes variability and ensures that the contact surfaces are prepared under identical conditions, thereby enhancing the reliability of the experimental results. The test was repeated 12 times under the current-carrying conditions of the moving and static contacts, and the voltage and current signals at the time of arcing were recorded and averaged to minimize the error. The tests were repeated 12 times to ensure the reliability and statistical significance of the results. This number was determined based on preliminary trials and statistical power analysis, which indicated that 12 repetitions would provide a sufficient sample size to capture variability and ensure the robustness of the findings. By repeating the tests multiple times, we can minimize the impact of random errors and enhance the confidence in the observed trends and conclusions.

Table 2. Parameters related to contacts.

Name	Material	Length (mm)	Diameter (mm)
moving contact	copper tungsten	30	20
static contact	copper tungsten	20	20

Figure 3. Contacts in kind.

2.3.2. Experimental Program Design

In this experiment, the effects of the sliding speed and contact pressure on arc generation in the current-carrying friction of OLTC contacts were investigated using a single-factor test method. The experiments included adjusting the sliding speed (30–120 mm/s) and contact pressure (0.7–2 N), recording the arc voltage, current and energy, observing the contact surface damage, and calculating the relevant parameters. Each group of tests was repeated 12 times to ensure consistent contact surface treatment [32].

3. Results

3.1. Effect of Sliding Speed on the Arc

3.1.1. Effect of Sliding Speed on Arc Voltage Waveforms

In the OLTC simulation test, the contact time of the dynamic/static contacts is shortened with an increase in sliding speed, resulting in a change in the arc voltage waveform. The contact state changes from static to dynamic with significant resistance fluctuations, affecting the arc generation and disappearance process. Voltage fluctuations and contact wear intensify with increasing speed, as shown in Figure 4. Faster sliding speeds may shorten the arc duration and increase the voltage peak, while slower sliding speeds prolong the arc duration and decrease the voltage peak. As the sliding speed increases, the dynamic interaction between contacts becomes more erratic, leading to greater voltage fluctuations and intensified wear due to increased mechanical vibrations and instability in the electrical contact. Faster speeds reduce the time contacts remain engaged, causing shorter arc durations and higher voltage peaks, while slower speeds allow a longer contact engagement, resulting in prolonged arc durations and lower voltage peaks.

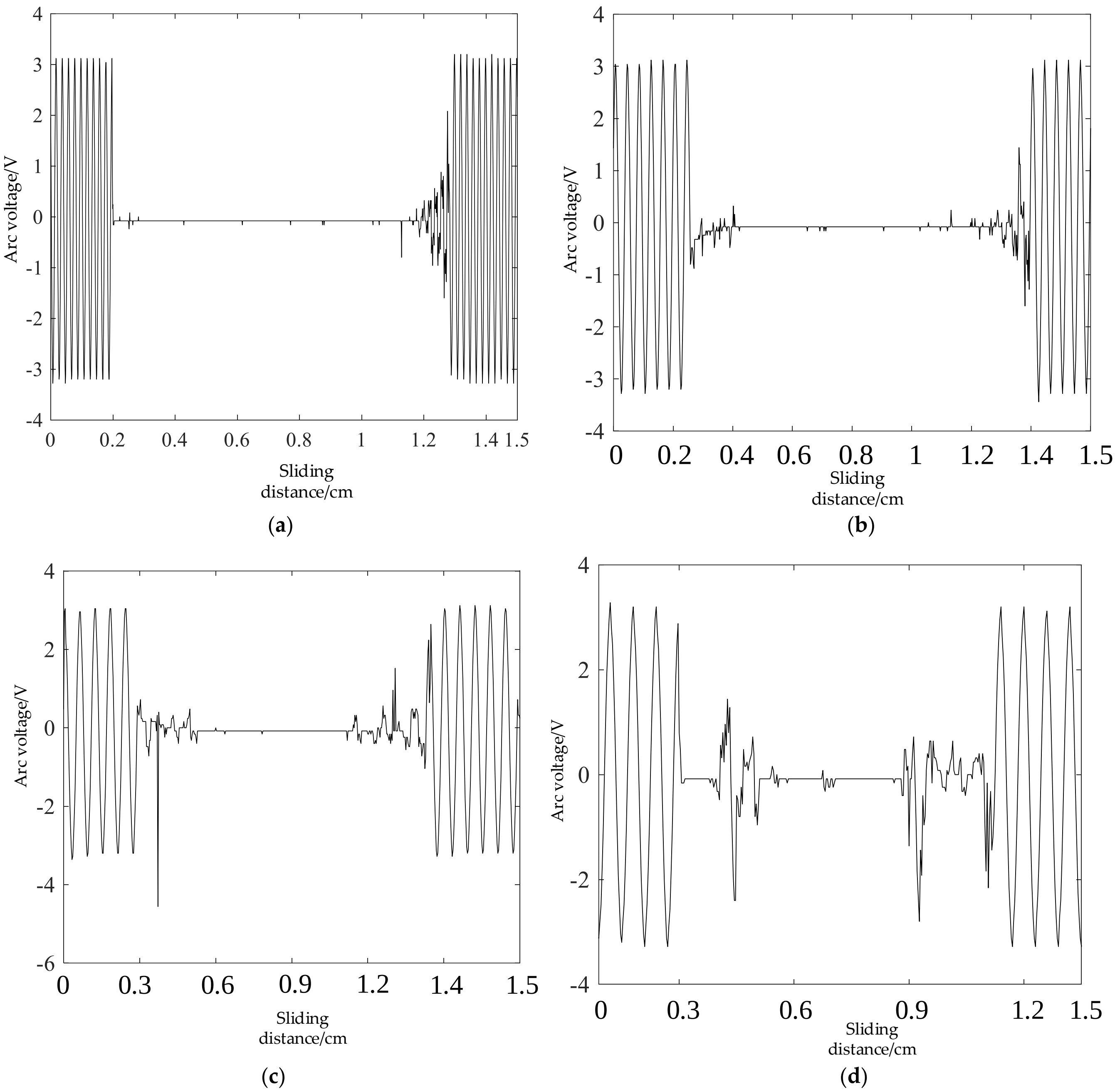

(**a**) (**b**) (**c**) (**d**)

Figure 4. Effect of sliding speed on voltage waveform. (**a**) v = 30 mm/s; (**b**) v = 60 mm/s; (**c**) v = 90 mm/s; (**d**) v = 120 mm/s.

3.1.2. Effect of Sliding Speed on Arc Energy

As shown in Figure 5, under 2 kV voltage, the arc energy changes with the sliding speed in an N-shaped trend, and the arc energy is larger when the contact pressure is small. When the sliding speed is 30–60 mm/s, the arc energy rises; when it is 60–120 mm/s, the arc energy decreases and then rises, and it is lowest when it is 90 mm/s. The arc duration decreases and then rises with the sliding speed, and the arc energy increases with the sliding speed. The arc duration shows a decreasing and then increasing trend with the sliding speed. The N-shaped trend in arc energy with sliding speed is likely due to the complex interplay between contact dynamics and electrical discharge behavior: at lower speeds (30–60 mm/s), increased friction and contact instability lead to higher arc energy, while at intermediate speeds (60–90 mm/s), improved contact stability reduces arc energy; however, at higher speeds (90–120 mm/s), increased vibration and a reduced contact time again elevate arc energy. This pattern reflects the balance between mechanical and electrical factors affecting arc formation and duration.

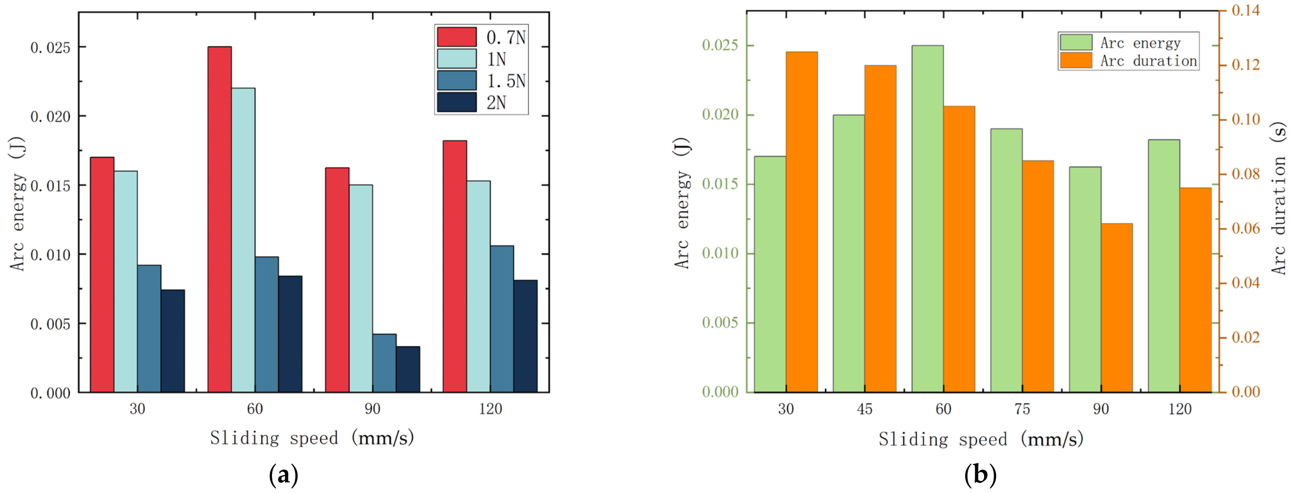

Figure 5. Effect of sliding speed on arc energy. (**a**) Arc energy at different sliding speeds; (**b**) arc energy and arc duration at different sliding speeds.

3.1.3. Effect of Sliding Speed on Arc Initiation Rate and Arc Resistance

Table 3 shows that the arc initiation rate increases and then decreases with an increase in sliding speed, showing an N-shaped change, which is consistent with the trend in arc energy. When the speed is 60–90 mm/s, the arc is pulled off rapidly and the arc initiation rate decreases; when it exceeds 90 mm/s, the vibration increases and the arc initiation rate rises. Meanwhile, the trend in arc resistance change is similar to the arc energy, and the speed increase leads to the arc resistance increase and the contact quality decrease. The speed increase causes the arc voltage fluctuation to increase and the arc current to decrease.

Table 3. Arcing rate and contact resistance at different sliding speeds.

Sliding Speed	Arc initiation Rate	Negative Bias	Positive Bias	Arc Resistance	Negative Bias	Positive Bias
30 mm/s	13.80%	1.4%	1.5%	1.55 Ω	0.4 Ω	0.5 Ω
60 mm/s	21.18%	1.4%	1.5%	1.72 Ω	0.4 Ω	0.5 Ω
90 mm/s	19.30%	1.3%	1.5%	1.67 Ω	0.3 Ω	0.5 Ω
120 mm/s	32.73%	1.5%	1.5%	3.16 Ω	0.5 Ω	0.5 Ω

3.2. Effect of Contact Pressure on the Arc

3.2.1. Effect of Contact Pressure on Arc Voltage Waveforms

As shown in Figure 6, increasing the contact pressure can effectively reduce the amplitude and frequency of voltage fluctuations at both ends of the contact and improve voltage stability. After the contact pressure reaches 1.5 N, the voltage change tends to stabilize. A larger contact pressure reduces contact resistance and arc generation, reducing the energy loss and wear of equipment.

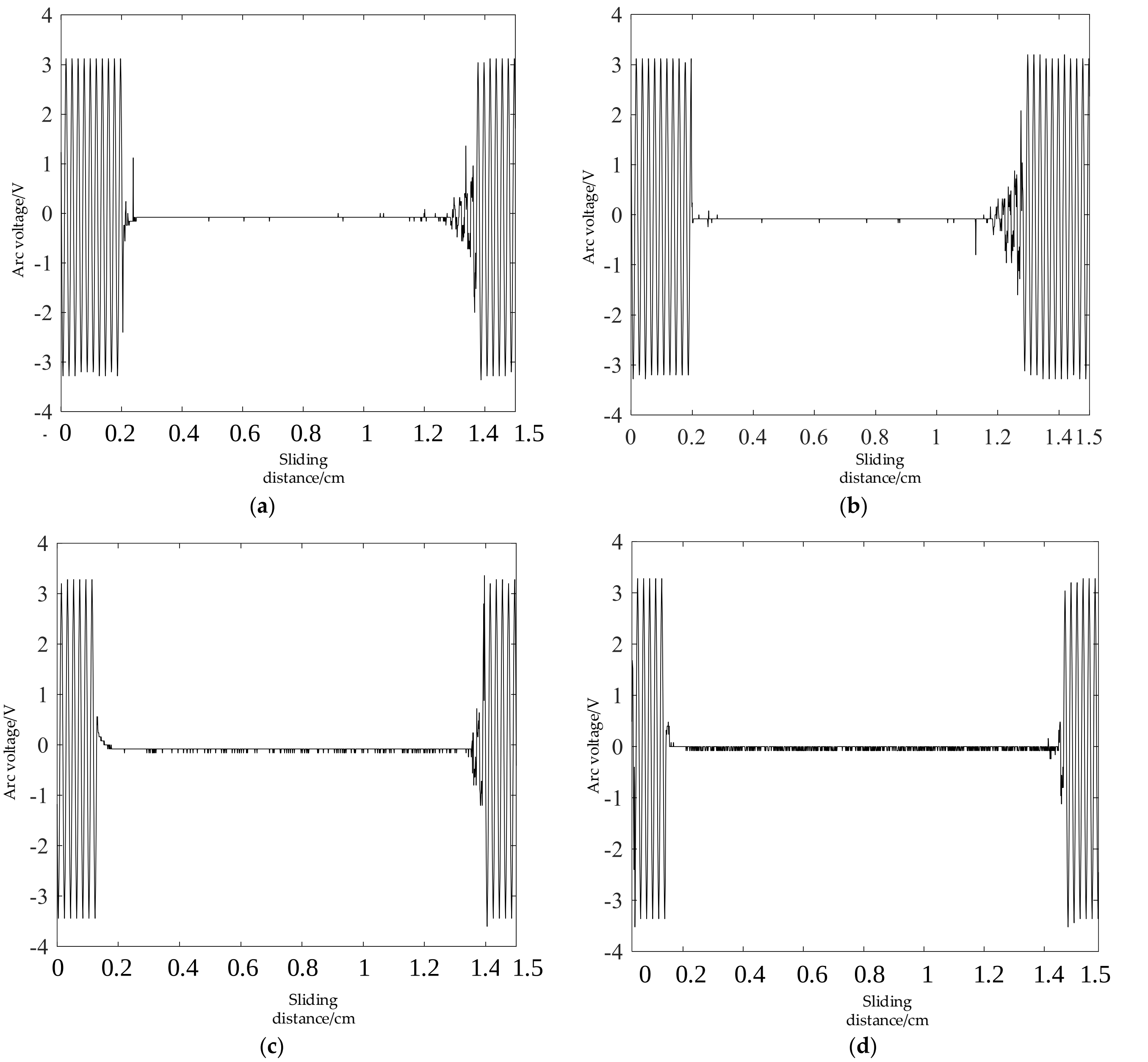

Figure 6. Effect of contact pressure on arc voltage waveforms. (**a**) F = 0.7 N; (**b**) F = 1 N; (**c**) F = 1.5 N; (**d**) F = 2 N.

3.2.2. Effect of Contact Pressure on Arc Energy Waveforms

The effect of contact pressure on the arc energy waveform is shown in Figure 7; the arc energy decreases with an increase in contact pressure, and when the contact pressure exceeds 1.5 N, this decrease decreases and the change tends to be stable. The arc duration also decreases with increasing contact pressure. Increasing the contact pressure improves the contact quality of the contacts, reduces the generation and intensity of the arc, and thus effectively suppresses the arc discharge frequency [33].

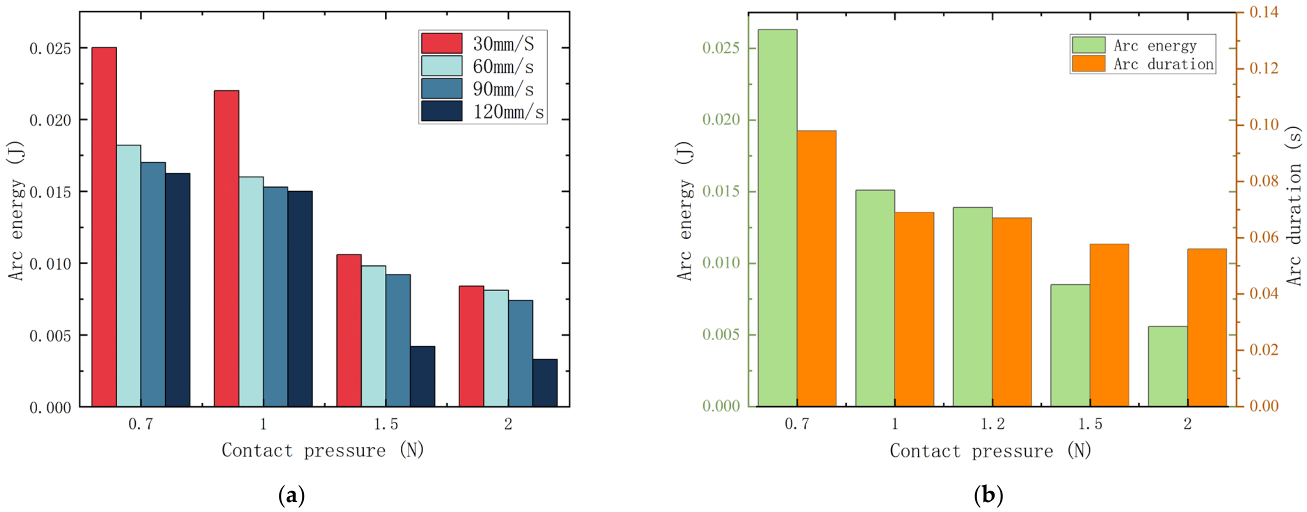

Figure 7. Effect of contact pressure on arc energy. (**a**) Arc energy at different contact pressures; (**b**) arc energy and arc duration at different contact pressures.

3.2.3. Effect of Contact Pressure on Arc Initiation Rate and Arc Resistance

Table 4 shows that the arc initiation rate and arc resistance decrease with increasing contact pressure, and the decreasing trend slows down after 1 N. Increased contact pressure reduces the friction oscillation shock between contacts and improves the contact conductivity and stability. The contact area is limited, the contact spot radius increases after the pressure increases, and the contact resistance becomes smaller, but this trend tends to stabilize.

Table 4. Arcing rate and contact resistance at different contact pressures.

Contact Pressure	Arc Initiation Rate	Negative Bias	Positive Bias	Arc Resistance	Negative Bias	Positive Bias
0.7 N	9.65%	0.4%	0.5%	3.06 Ω	0.1 Ω	0.2 Ω
1 N	6.95%	0.4%	0.5%	1.8 Ω	0.1 Ω	0.2 Ω
1.2 N	6.26%	0.3%	0.5%	1.59 Ω	0.1 Ω	0.2 Ω
1.5 N	4.77%	0.5%	0.5%	1.30 Ω	0.1 Ω	0.2 Ω
2 N	3.53%	0.4%	0.5%	1.03 Ω	0.1 Ω	0.2 Ω

4. Discussion

According to the experimental data, we explore the impact of the sliding speed and contact pressure on the arc and construct the relevant objective function, using of the nonlinear regression method to establish the functional relationship between the sliding speed and contact pressure and arc energy, and by comparing and analyzing the trend in the experimental data, the selection of appropriate operating parameters to reduce the generation of the arc has a positive inhibition; for this reason, the objective function of minimizing arc energy is established, which includes the function of the sliding speed and arc energy and the function of contact pressure and arc energy, and the range of the most suitable sliding speed is finally determined.

4.1. Construction of the Arc Energy Function

4.1.1. Multivariate Nonlinear Regression

In the context of current-carrying conditions, the variation in arc energy is influenced by multiple factors, including contact current, load, and sliding speed, all of which exhibit a nonlinear relationship. To thoroughly analyze the impact of these factors on arc energy changes, a multivariate nonlinear regression approach is essential. The process involves the following steps:

1. A Selection of the Function Type and Regression Model: Based on the nature of the problem and the characteristics of the data, an appropriate nonlinear model is selected to ensure the accuracy and reliability of the regression.
2. An Estimation of Unknown Parameters: The nonlinear regression curve is transformed into a linear regression line through variable substitution. This transformation allows for the estimation of model parameters using linear regression techniques.
3. The Application of Linear Regression for the Prediction: Linear regression methods are employed to construct prediction equations, facilitating the forecasting of outcomes based on the model.
4. An Inverse Operation for a Nonlinear Regression Equation: Using the estimated parameters, the model is fitted to derive the final multivariate nonlinear regression model, providing a comprehensive representation of the data.
5. An Evaluation of Model Effectiveness and Accuracy: The fitted model is assessed using residual analysis, R^2, and other metrics to evaluate its fit and predictive capability. The correlation coefficient R^2 is particularly important as it quantifies the degree to which the predicted data align with the observed data, indicating the model's effectiveness.

The correlation coefficient R^2 was introduced to describe the degree of fit of the predicted data to the observed data, as shown in Equation (1).

$$R^2 = 1 - \frac{\sum_{t=1}^{N} (y_\text{t} - \hat{y}_\text{t})^2}{\sum_{t=1}^{N} (y_\text{t} - \overline{y})^2}, \tag{1}$$

where y_t is the measured value; $\hat{y}_t$ is the predicted value; and $\overline{y}_t$ is the mean value. The larger the R^2, the better the fit.

4.1.2. Construction of the Objective Function

During the OLTC operation, the size of the arc is mainly affected by the sliding speed and contact pressure. The sliding speed affects the length and energy density of the arc, while the contact pressure affects the shape and stability of the arc. Therefore, the limiting effects of these two factors need to be considered when establishing the functional relationship of arc energy. In order to minimize the arc energy, the appropriate sliding speed and contact pressure conditions need to be selected. In practice, through the establishment of the sliding speed and arc energy as a function of contact pressure and arc energy and through the use of multiple nonlinear regression analysis, we build a complex model between the sliding speed and contact pressure and arc energy so as to predict the rule of change in arc energy under specific conditions.

In order to ensure the safe and stable operation of the equipment, some constraints, such as the maximum allowable arc energy, are usually set. Therefore, it is crucial to seek the minimum value of arc energy within these constraints. Through the model established by the multiple nonlinear regression analysis, the combination of sliding speed and contact pressure that minimizes the arc energy under specific constraints can be found to achieve the best operating results, and then the objective function is as follows:

$$E(x) = \begin{cases} \min E_1(x_1), E_2(x_2) \text{at the minimum} \\ \min E_2(x_2), E_1(x_1) \text{at the minimum}' \end{cases} \tag{2}$$

where E(x) is the magnitude of arc energy in J during the operation; $E_1(x_1)$ is the magnitude of arc energy in J at different sliding speeds; $E_2(x_2)$ is the magnitude of arc energy in J at different contact pressures; x_1 represents the magnitude of the sliding speed in mm/s; and x_2 represents the magnitude of contact pressure in N.

4.2. Sliding Speed as a Function of Arc Energy

Arc tests at different sliding speeds are performed by the OLTC simulation test device, and arc energy data can be obtained, as shown in Tables 5–8. These data support subsequent analysis and modeling to help understand the performance of the OLTC under different operating conditions and provide a reference for optimizing the design. The experimental data can also be used to verify the accuracy of the simulation modeling and improve the design and operation efficiency of the OLTC. Selecting the data that only change the sliding speed for analysis, the fitting analysis of the experimental data by software such as MATLAB can find the functional relationship between the sliding speed and the arc energy. This fitting analysis reveals the nonlinear influence law of sliding speed on arc energy.

Table 5. Test data at sliding speed 30 mm/s.

Group	Arc Current (A)	Arc Voltage (V)	Arc Energy (J)
1	0.296	0.8	0.032
2	0.032	0.8	0.005
3	1.069	1.44	0.373
4	0.696	0.52	0.026
5	0.304	0.44	0.013
6	0.02	1.32	0.002
7	0.45	0.39	0.016
8	0.31	0.68	0.027

Table 6. Test data at sliding speed 60 mm/s.

Group	Arc Current (A)	Arc Voltage (V)	Arc Energy (J)
1	0.5	0.32	0.018
2	0.62	0.3	0.017
3	0.98	0.72	0.049
4	0.12	0.64	0.011
5	0.24	0.4	0.019
6	0.54	0.52	0.024
7	0.59	0.32	0.047
8	0.3	0.315	0.054

Table 7. Test data at sliding speed 90 mm/s.

Group	Arc Current (A)	Arc Voltage (V)	Arc Energy (J)
1	0.0354	0.68	0.016
2	0.0354	0.52	0.009
3	0.0354	0.48	0.01
4	0.0354	0.72	0.025
5	0.0354	0.68	0.014
6	0.134	0.44	0.005
7	0.13	0.417	0.004
8	0.142	0.4	0.004

Table 8. Test data at sliding speed 120 mm/s.

Group	Arc Current (A)	Arc Voltage (V)	Arc Energy (J)
1	0.356	1.36	0.023
2	0.154	1.44	0.01
3	0.154	1.24	0.009
4	0.256	0.64	0.011
5	0.118	1.44	0.01
6	0.384	1.48	0.068
7	0.376	0.68	0.031
8	0.32	1.52	0.039

By screening and analyzing the above experimental data, the value of arc energy under a specific sliding speed can be finally calculated as 0.017 J. This value can reflect the degree of influence of the sliding speed on the arc energy under the experimental conditions. By observing and analyzing the change in arc energy with the sliding speed, it can be found that the change in arc energy is disordered, which indicates that in the process of sliding, the change in arc energy has a certain degree of randomness and complexity. This disordered change also reflects the complex change trend in the arc in practice, which provides an important experimental data base for a further study of the arc behavior.

By screening the above test data, the final value of the arc energy was calculated to be 0.025 J.

By screening the above test data, the final value of the arc energy was calculated as 0.01625 J.

By screening the above test data, the final value of arc energy was calculated as 0.0182 J.

Analyzing the above data, when the contact pressure and other parameters are unchanged, the arc energy between the contacts changes with an increase in the sliding speed. The experimental data show that the arc energy with an increase in the sliding speed shows a trend of first increasing, then decreasing and then increasing. This trend indicates that the effect of the sliding speed on arc energy is not a simple linear relationship but may be affected by a combination of factors. Considering the efficiency and damage problems of an OLTC during operation, this paper will focus on analyzing the change in the latter half of the curve in order to better understand the influence law of the sliding speed on arc energy under actual working conditions. Through the fitting of MATLAB R2023b (9.13) software, the functional relationship between the two can be derived as

$$E_1(x_1) = 5.944\text{e} - 06x_1^2 - 0.001183x_1 + 0.0746, \tag{3}$$

Considering the goodness of fit of the function equation R^2 = 1, the calculation of Equation (3) found that there exists a minimum value of $E_1(x_1)$, and when sliding speed x_1 is 99.512 mm/s, there is a value of 0.0157 J. Thus, it is seen that within the interval of 30 mm/s to 120 mm/s, there exists a sliding speed whereby the contact friction movement generated by the arc of the contacts has the smallest possible impact on the contacts.

4.3. Contact Pressure as a Function of Arc Energy

Analyzing the experimental data, it is found that an increase in contact pressure within a certain range will correspondingly increase the arc energy. This is because the appropriate contact pressure improves the contact area between the contacts and reduces the contact resistance, thus reducing the arc energy loss and improving the energy transfer efficiency. However, too large a contact pressure further reduces the contact resistance but increases the friction and wear, resulting in the premature wear and damage of the contacts, and this even leads to arc instability or bounce, affecting the operation of the equipment. On the contrary, too small a contact pressure reduces friction and wear but increases the contact resistance, resulting in increased arc energy loss, reduced energy transfer efficiency, and even arc instability. Therefore, in design and use, it is necessary to choose the appropriate contact pressure according to the specific situation to balance the energy transfer efficiency and equipment life. In the case of other factors such as sliding speed and other factors, they remain unchanged, but there is a change in the contact pressure, and the relevant data changes are shown in Figures 8–12.

In Figures 8–12, the experimental data clearly indicate that an increase in contact pressure leads to a more stable voltage and current trend, reducing fluctuations. This suggests the enhanced stability of electrical characteristics. Moreover, processing the data in these figures shows a significant decrease in arc energy with increased contact pressure. When the pressure is 1 N, 1.2 N, 1.5 N, and 2 N, the arc energy measures 0.0263 J, 0.0151 J, 0.0139 J, 0.0085 J, and 0.0056 J, respectively.

Through calculations and analysis, as the contact pressure increases, the probability of arc generation between contacts decreases, the current-carrying efficiency rises, the arc energy decreases, and the oscillation between contact friction vices decreases. The relationship between contact pressure and arc energy is further analyzed and the functional relationship between the two is derived as

$$E_2(x_2) = 0.01312x_2^2 - 0.05068x_2 + 0.05465, \quad (4)$$

In the interval of contact pressure from 0.7 N to 2 N, $E_2(x_2)$ decreases as the contact pressure x_2 increases, and the goodness of fit of the functional equation is R^2 = 0.9734. The changes in contact pressure and arc energy are negatively correlated.

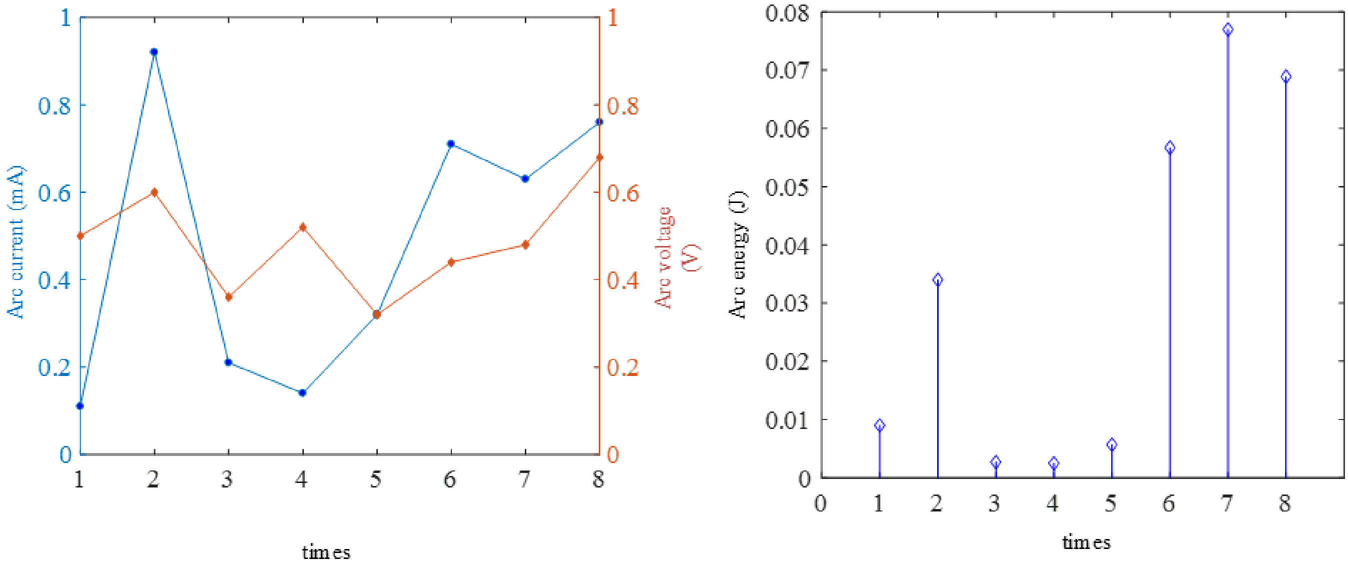

(**a**) (**b**)

Figure 8. Contact pressure F = 0.7 N. (**a**) Change in voltage and current; (**b**) change in arc energy.

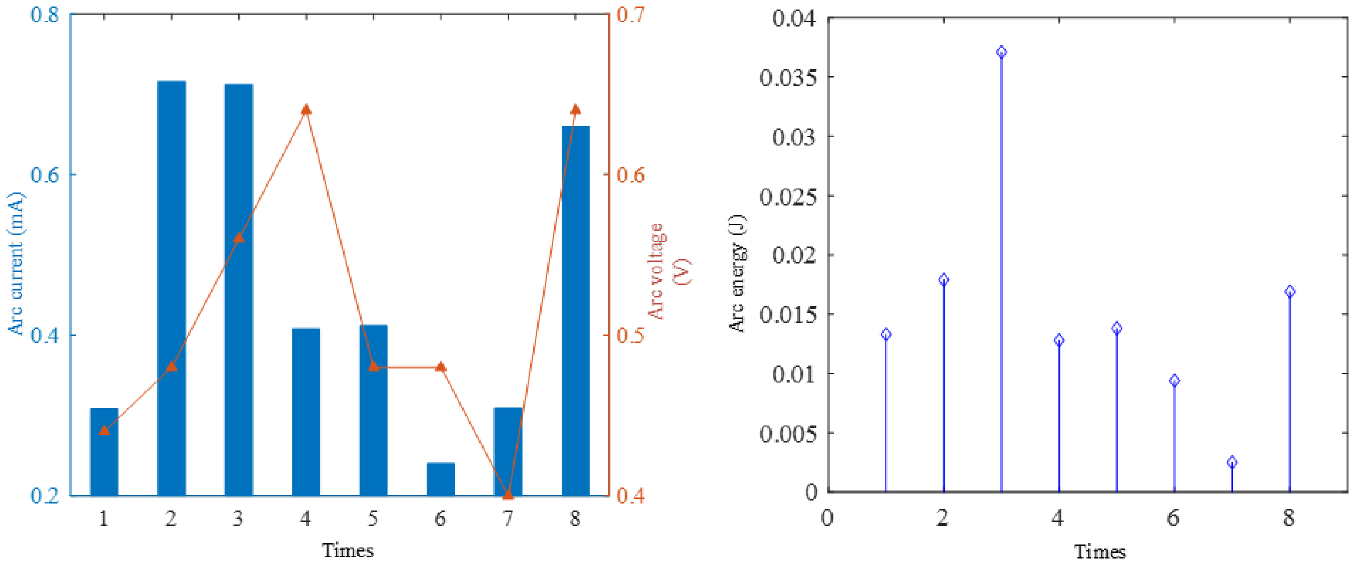

(**a**) (**b**)

Figure 9. Contact pressure F = 1 N. (**a**) Change in voltage and current; (**b**) change in arc energy.

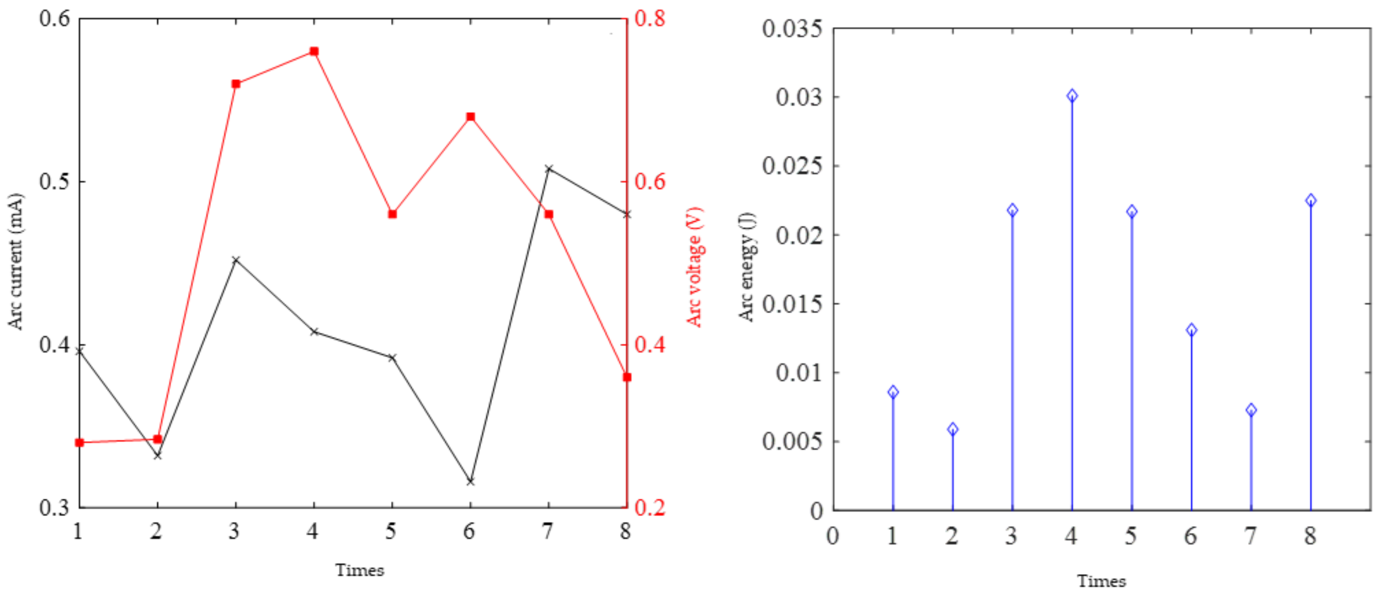

(a) **(b)**

Figure 10. Contact pressure F = 1.2 N. (**a**) Change in voltage and current; (**b**) change in arc energy.

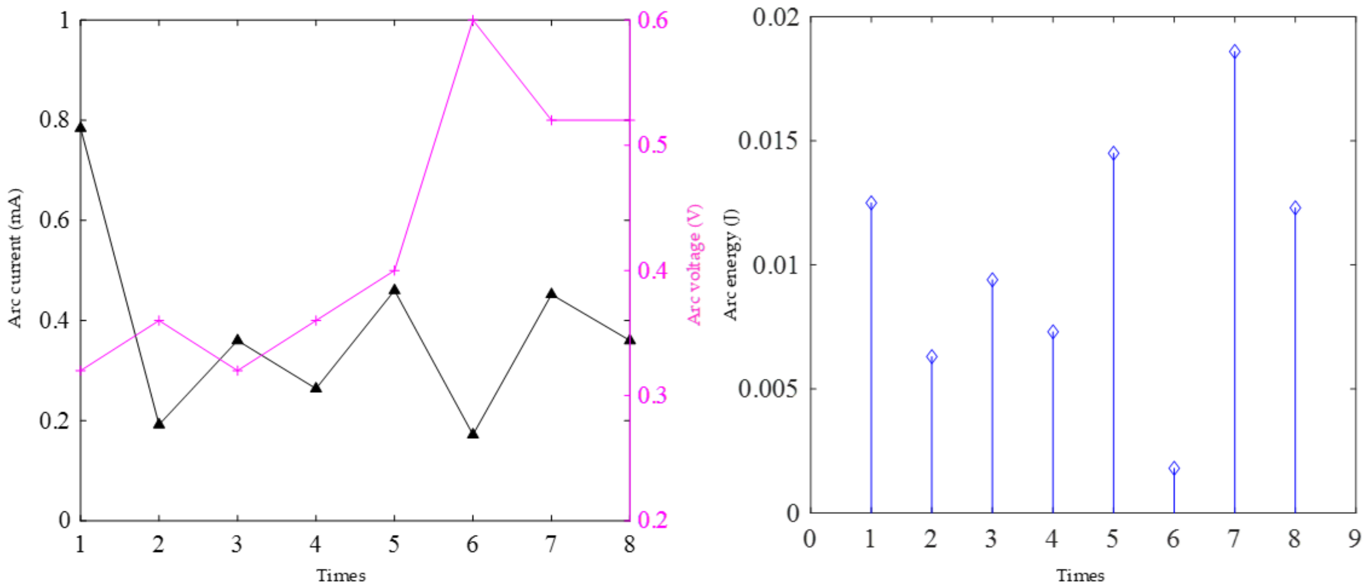

(a) **(b)**

Figure 11. Contact pressure F = 1.5 N. (**a**) Change in voltage and current; (**b**) change in arc energy.

4.4. Range of Optimal Sliding Speed

By comparing and analyzing the expressions for sliding speed and contact pressure as a function of arc energy, it is found that both satisfy the following nonlinear expression:

$$E_i(x_i) = ax_i^2 + \mathrm{b}x_i + c \tag{5}$$

4.4.1. Sliding Speed as a Function of Arc Energy at Different Contact Pressures

In order to further investigate the functional relationship between sliding speed and arc energy, the sliding speed and arc energy under different contact pressures were analyzed. The functional relationship between sliding speed and arc energy under different contact pressures is shown in Table 9, where $30 \leq x_1 \leq 120$.

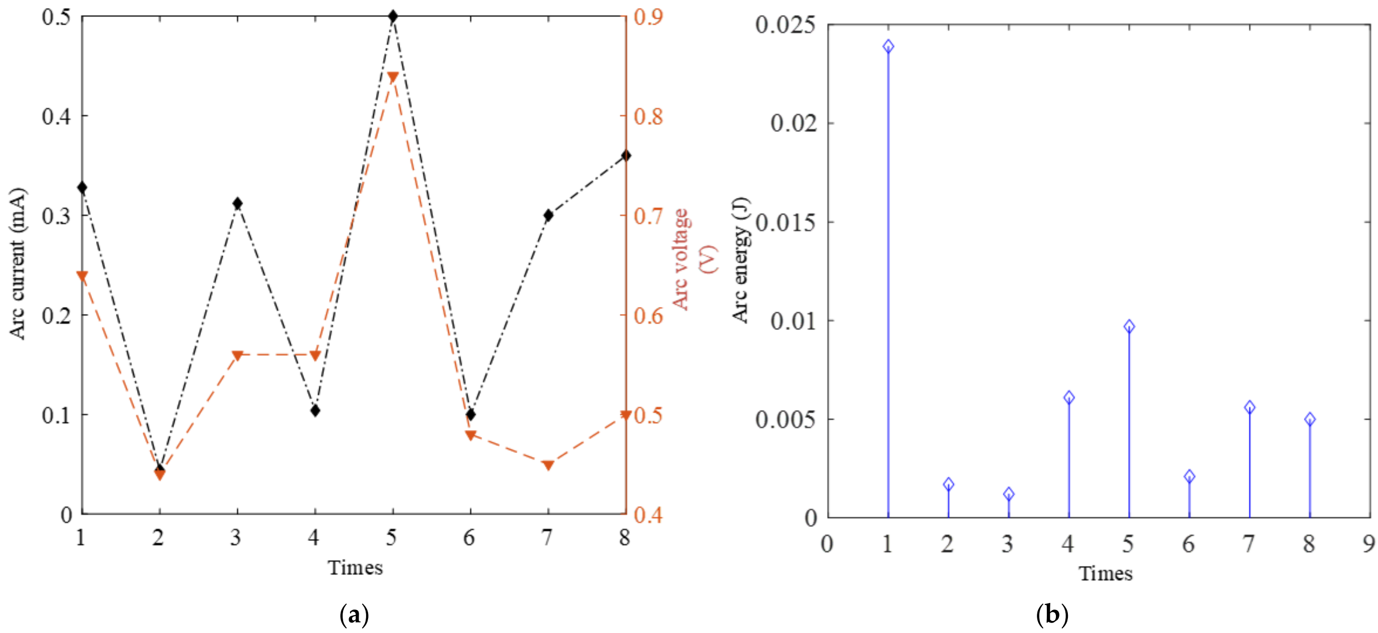

Figure 12. Contact pressure F = 2 N. (**a**) Change in voltage and current; (**b**) change in arc energy.

Table 9. Parameter table for different sliding speeds and arc energy expressions for specific contact pressures.

Contact Pressure	a	b	c	Minimum Arc Energy	Corresponding Sliding Speeds	R^2
0.7 N	5.944×10^{-6}	−0.001183	0.0746	0.0157 J	99.51 mm/s	1
1 N	4.056×10^{-6}	−0.0008417	0.0579	0.0142 J	103.75 mm/s	1
1.5 N	6.667×10^{-6}	−0.001187	0.057	0.0042 J	89.02 mm/s	1
2 N	5.5×10^{-6}	−0.000995	0.0483	0.0033 J	90.45 mm/s	1

Through the above comparison, it is found that under different contact pressures, the sliding speed value that minimizes the arc energy when the contact is running is about 90 mm/s. Combined with Figure 5 and the sliding speed value corresponding to the above minimum arc energy, it is concluded that the optimal range of the contact sliding speed of the OLTC is 89–103 mm/s.

Under different sliding speeds, the effects of different contact pressures on the change in arc energy are consistent, and all of them decrease gradually. At the same time, combined with the wear of contact pressure on the contact surface seen in Table 3, it can be introduced that contact pressure can minimize the impact of the arc on the friction side of the OLTC contacts when the value of the contact pressure is in the range of 1.5 N.

4.4.2. Contact Pressure as a Function of Arc Energy for Different Sliding Speeds

The functional relationship between contact pressure and arc energy at different sliding speeds is analyzed, and the parameters obtained by fitting reflect the complex relationship between contact pressure and arc energy. These functional relationships can be used to predict the relationship between contact pressure and arc energy at different sliding speeds, which provides an important reference for optimizing the contact parameters and improving the contact quality of sliding contacts. The functional relationship equations between contact pressure and arc energy at different sliding speeds are obtained as shown in Table 10, where ($0.7 \leq x_2 \leq 2$).

Table 10. Parameter table for different contact pressures and arc energy expressions for specific sliding speeds.

Contact Pressure	a	b	c	R^2
30 mm/s	0.002209	−0.01413	0.02649	0.9458
60 mm/s	0.008088	−0.03596	0.0474	0.9469
90 mm/s	0.005609	−0.02653	0.03332	0.9123
120 mm/s	0.003012	−0.01604	0.02808	0.9981

Analyzing Table 10, it is found that at different sliding speeds, the effects of different contact pressures on the change in arc energy are consistent, and all of them decrease gradually, and it can be introduced that the contact pressure can minimize the effect of the arc on the friction vice of the OLTC contact when it takes a range of values near 1.5 N.

4.4.3. Optimal Sliding Speed and Contact Pressure Under Minimum Arc Energy Constraints

In order to further investigate the effects of the sliding speed and contact pressure on the arc of OLTC contacts, the effects of sliding speed and contact pressure on arc energy need to be considered together to achieve an optimal OLTC contact design. The relationship between sliding speed and contact pressure and arc energy is analyzed by a correlation, and the relationship between the two and arc energy is fitted to a surface, and the following results are obtained, as shown in Figure 13.

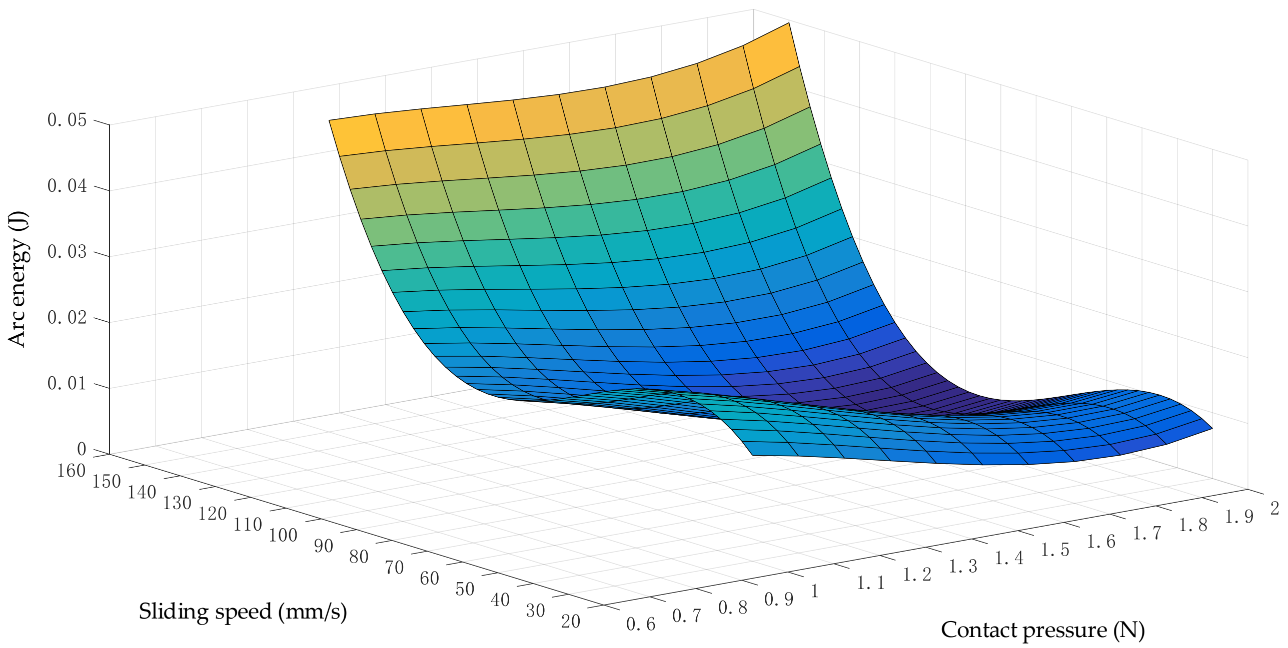

Figure 13. Variation in arc energy at different contact pressures and different sliding speeds.

By analyzing Figure 13, considering the trend of arc energy with the sliding speed and contact pressure and comparing the effects of different speeds and different contact pressures on arc energy and contact surface morphology, it is concluded that the operating parameter conditions that can minimize the effects of an arc on the OLTC sliding contacts are as follows: the sliding speed ranges from 89 to 103 mm/s, and contact pressure ranges from 1.5 to 1.7 N. The contact pressure is between 1.5 and 1.7 N.

5. Conclusions

In order to solve the lack of the quantification of arc influencing factors in the oil medium of an oil-immersed OLTC and the unclear limiting range of influencing factors for arc suppression by dynamic and static contacts, this paper draws the following conclusions through the design of an optimal sliding speed by means of the multivariate nonlinear regression method:

1. An arc test platform simulating the contact mode of oil-immersed OLTC movable and static contacts is built to provide data samples for exploring the relationship between the sliding speed and contact pressure and arc energy by simulating different sliding speeds and contact pressures in the test.
2. In the range of contact pressure from 0.7 to 2 N, the arc energy increases and then decreases with an increase in the sliding speed; in the range of sliding speeds from 30 to 120 mm/s, the arc energy decreases with an increase in contact pressure.
3. Under different contact pressures, the sliding speed value that minimizes the arc energy during contact operation is about 90 mm/s, and the optimal range of the contact sliding speed for the OLTC is 89–103 mm/s.
4. Through the multivariate nonlinear regression analysis, the operating parameters that minimize the impact of the arc on the OLTC sliding contacts are as follows: a sliding speed in the range of 89–103 mm/s and contact pressure in the range of 1.5–1.7 N.

As the simulated arc experimental platform can simulate the actual contact friction of the movable and static contacts, the optimal sliding speed and contact pressure range analyzed in this paper can be put into actual engineering use. In contrast to previous studies that primarily focus on the qualitative analysis of arc behavior in OLTCs, this study quantitatively determines the optimal sliding speed and contact pressure ranges—89–103 mm/s and 1.5–1.7 N, respectively—using a multivariate nonlinear regression approach. This methodological advancement allows for a more precise control of arc energy, reducing wear and extending the service life of OLTCs. This article provides guidance and references for selecting materials, designing shapes, and establishing operating standards for moving and stationary contacts.

Author Contributions: Conceptualization, Z.X. and S.Z.; data curation, J.Z. and X.W.; formal analysis, J.Z. and Y.X.; funding acquisition, Z.X.; investigation, Z.L. and M.M.; methodology, S.Z. and Z.L.; project administration, Z.X. and S.L.; resources, S.L.; software, S.Z. and J.Z.; supervision, Z.X. and S.L.; validation, X.W., Y.X., Z.L. and M.M.; visualization, Z.X. and S.Z.; writing—original draft preparation, Z.X.; writing—review and editing, Z.X., S.Z. and J.Z. All authors have read and agreed to the published version of the manuscript.

Funding: This research was funded by the Scientifical Project of State Grid Gansu Guangming Electric Power Engineering Consulting and Supervision Co., Ltd., grant number SGGSJL00JLWT2400321.

Data Availability Statement: The data included in this paper are available upon request.

Conflicts of Interest: Author Zhiqi Xu, Sijiang Zhang, Jintao Zhang, Xiaobing Wang and Yanwen Xu were employed by the company GanSu Guangming Electric Power Engineering Consulting and Supervision Co., Ltd. Li Zongying, Ma Minghan, and Li Shuabing are affiliated with the School of New Energy and Power Engineering at Lanzhou Jiaotong University. ALL authors declare that the research was conducted in the absence of any commercial or financial relationships that could be construed as a potential conflict of interest.

References

1. Yang, X. Evolution Mechanism of Contact Resistance of Oil-Immersed On-Load Tap-Changer. Master's Thesis, Lanzhou Jiaotong University, Lanzhou, China, 2013.
2. Plesca, A. Thermal analysis of sliding electrical contacts with mechanical friction in steady state conditions. *Int. J. Therm. Sci.* **2014**, *84*, 125–133. [CrossRef]
3. Yu, X.; Song, M.; Wang, Z. Simulation study on surface temperature distribution of collector strip material under pantograph-catenary arc of urban rail. *IEEE Access* **2023**, *11*, 68358–68365. [CrossRef]

4. Li, Y.; Li, W.; Han, T.; Zheng, X.; Li, J.; Li, B.; Fan, S.; Qiu, C.-W. Transforming heat transfer with thermal metamaterials and devices. *Nat. Rev. Mater.* **2021**, *6*, 488–507. [CrossRef]
5. Wu, G.; Dong, K.; Xu, Z.; Zheng, X.; Li, J.; Li, B.; Fan, S.; Qiu, C.-W. Pantograph–catenary electrical contact system of high-speed railways: Recent progress, challenges, and outlooks. *Railw. Eng. Sci.* **2022**, *30*, 437–467. [CrossRef]
6. Zeng, Q.; Wang, F.; Zheng, Y.; He, W. Fault identification of transformer on-load tap-changer based on convolutional neural network. *Power Syst. Cust.* **2020**, *44*, 144–151.
7. Zhang, D. Current situation and development trend of OLTC in China. *Transformer* **2001**, 144–151. [CrossRef]
8. Dong, L.; Chen, G.; Zhu, M.; Zhou, Z.R. Wear mechanism of aluminum-stainless steel composite conductor rail sliding against collector shoe with electric current. *Wear* **2007**, *263*, 598–603. [CrossRef]
9. Dong, L.; Li, F.; Chen, G.; Zhu, M. Friction and wear characteristics of steel-aluminum composite rail/current collector under current and non-current conditions. *Lubr. Seal.* **2006**, *6*, 36–38.
10. Fu, W.; Wu, Y.; Liu, L.; Chen, G. Effect of high current on current-carrying friction and wear properties of carbon sliders/copper-silver alloy contact lines. *Transformer* **2017**, *42*, 52–56.
11. Xing, Z. Analysis and Modeling of Strong Current Sliding Electric Contact Wear Characteristics. Master's Thesis, Liaoning Technical University, Fuxin, China, 2022.
12. Zhong, C.; Xu, Y.; Chen, G. Experimental study on current-carrying friction and wear properties of metallized carbon slide/copper-silver alloy contact line. *Transformer* **2021**, *46*, 34–39.
13. Ding, T.; Chen, G.; Bu, J.; Zhang, W.H. Effect of temperature and arc discharge on friction and wear behaviours of carbon strip/copper contact wire in pantograph–catenary systems. *Wear* **2011**, *271*, 1629–1636. [CrossRef]
14. Ding, T.; Chen, G.; Shen, M.X.; Zhu, M.H.; Zhang, W.H. Effect of arc discharge on friction and wear behaviors of stainless steel/copper-impregnated metalized carbon couple under electric current. *Adv. Mater. Res.* **2010**, *150–151*, 1364–1368. [CrossRef]
15. Ding, T.; Chen, G.; Zhu, Y. Effect of normal load on friction and wear properties of stainless steel/metal-impregnated carbon. *Mech. Eng. Mater.* **2021**, *46*, 34–39.
16. Shi, G.; Chen, Z.; Guo, G.; Hui, L.; Dang, W. Research on contact resistance characteristics and modeling of bow mesh under fluctuating load. *Trans. Electrotech. Soc.* **2019**, *34*, 2287–2295.
17. Chen, Z.; Wang, Y.; Yang, C.; Shi, G.; Hui, L. Study on dynamic contact resistance characteristics of bow mesh under fluctuating load. *High Volt. Electr. Appar.* **2019**, *55*, 148–155.
18. Wang, S.; Li, P.; Li, J.; Zhang, S.Q.; Wang, K.; Li, G.Q.; Li, G.; Xiao, Y. Review of research on transformer vacuum on-load tap-changer. *Proc. CSEE* **2022**, *42*, 6893–6908.
19. Zhang, S.; Zhang, Y.; Wang, K.; Zhang, N.; Xiao, Y.; Li, X.; Li, G.; Li, G. Dynamic modeling and simulation analysis of vacuum on-load tap-changer. *Proc. CSEE* **2023**, *43*, 3621–3630.
20. Wang, X.; Xiao, J.; Zhang, L.; Zhou, K. Effect of load on tribological and wear properties of AuNi9/gold coated friction pair. *Chin. J. Nonferrous Met.* **2023**, *22*, 3427–3431.
21. Chen, Z.; Gao, H.; Wang, X.; Xing, Z. Influence of friction vibration acceleration on pantograph catenary current carrying characteristics. In Proceedings of the 2022 2nd International Conference on Electrical Engineering and Mechatronics Technology (ICEEMT), Hangzhou, China, 1–3 July 2022; pp. 82–90.
22. Qu, C.; Chen, Z.; Ren, R.; Gao, H.; Tang, J. Analysis and modeling of frictional vibration characteristics of arch mesh under fluctuating load. *New Technol. Electr. Energy* **2021**, *40*, 29–38.
23. Yu, X.; Ma, Z.; Zhang, L.; Zhang, X.; Kang, X. Effect of load on friction and wear properties and stability of AuNi9/PdNi-Au friction pair. *Powder Metall. Mater. Sci. Eng.* **2022**, *27*, 648–658.
24. Liu, D.; Fan, J.; Dong, B.; Li, X.; Chen, G. Friction and wear properties of metal-impregnated carbon slide in rigid catenary under different normal loads. *Lubr. Seal.* **2023**, *48*, 89–94.
25. Yang, Z.; Song, Y.; Jiao, J.; Li, W.; Shangguan, B.; Zhang, Y. Optimization of current-carrying friction and wear properties of copper-carbon composite materials based on damage. *Tribol. Int.* **2023**, *191*, 109074. [CrossRef]
26. Dong, B.; Hu, Y.; Chen, G.; Huang, H.; Wu, Y.; Cui, X.; Gao, G.; Wu, G. Experimental study on arc discharge and temperature rise of carbon slide in current-carrying friction of pantograph/catenary. *Lubr. Seal.* **2016**, *41*, 41–45.
27. Yang, H.; Chen, G.; Gao, G.; Wu, G.N.; Zhang, W.H. Experimental research on the friction and wear properties of a contact strip of a pantograph–catenary system at the sliding speed of 350 km/h with electric current. *Wear* **2015**, *332*, 949–955. [CrossRef]
28. Liu, Z.; Liu, Z.; Du, H. Cu-based powder metallurgy/Q235B friction pair current-carrying friction and wear properties. *Lubr. Seal.* **2022**, *47*, 176–184.
29. Li, J.; Zhang, Y.; Song, C.; Sun, Y.; Chen, T.; Zhang, Y. Arc behavior and electrical damage of pure copper rolling current-carrying friction pair at different speeds. *J. Mech. Eng.* **2021**, *57*, 168–176.
30. Wang, D.; Chen, X.; Li, F.; Chen, W.; Li, H.; Yao, C. Influence of normal load, electric current and sliding speed on tribological performance of electrical contact interface. *Microelectron. Reliab.* **2023**, *142*, 114929. [CrossRef]
31. Luo, X. Study on Friction and Wear Characteristics and Contact Resistance of Sliding Current-Carrying Friction Pair with Rough Surface. Master's Thesis, Liaoning Technical University, Fuxin, China, 2021.

32. Li, Z.; Li, S.; Kang, Y.; Li, Z.; Li, H. Erosion characteristics of oil-immersed on-load tap changer contacts under varying contact speeds and pressures. *Chin. J. Electr. Eng.* **2024**, *10*, 21–34. [CrossRef]
33. Xu, Y.; Chen, G.; Zhong, C.; Yang, P. Current-carrying friction and wear properties of metallized carbon sliding plates with different copper content. *Lubr. Seal.* **2024**, *47*, 60–66.